High-resolution scanning force microscopy of gold nanoclusters on the KBr (001) surface

O. H. Pakarinen,[1,*] C. Barth,[2] A. S. Foster,[1] R. M. Nieminen,[1] and C. R. Henry[2]
[1]*Helsinki University of Technology, Laboratory of Physics, P.O. Box 1100, FIN-02015 HUT, Finland*
[2]*CRMCN-CNRS, Campus de Luminy, Case 913, 13288 Marseille Cedex 09, France*
(Received 7 October 2005; revised manuscript received 29 March 2006; published 23 June 2006)

In this study we use a combination of dynamic scanning force microscopy experiments and first-principles simulations to study the imaging process of gold nanoclusters adsorbed on the (001) surface of KBr. In previous experiments atomic resolution was readily obtained on the KBr substrate. However, it was not possible to resolve atoms within the clusters themselves. This correlates with imaging simulations we present here using several different probable tip models: measurable contrast was readily achieved on the KBr surface and on the gold (001) surface, but simulations on the clusters demonstrated poor contrast for all tips. We further consider the role of cluster charging in the tip-surface interaction, and the role that surface defects play in the properties of adsorbed clusters.

DOI: 10.1103/PhysRevB.73.235428 PACS number(s): 68.37.Ps, 61.46.−w, 68.43.Bc

I. INTRODUCTION

Much of the research into heterogeneous catalysis remains focused on the properties of small metal nanoclusters adsorbed onto surfaces of single oxide materials.[1] Although these model catalytic systems are far from the real industrial systems, they can provide great insight into the nature of the fundamental reactions at the heart of the catalytic process. Due to their particular relevance as replacements for Pt- or Pd-based catalytic converters in car exhausts, many recent studies have focused on studying the reactivity of small gold clusters.[2–14] These gold nanoclusters are catalytically active only when the size of the cluster is less than about 4 nm. The reason for this increased reactivity remains controversial.[15] The most recent results suggest that primarily the low-coordinated atoms are bonding sites for CO and O_2,[9,16–19] and that the interaction with the substrate[14,20] or charge transfer could also play a role in the catalysis by gold clusters.[12,13]

Scanning probe microscopy offers an excellent possibility for *in situ* studies of the properties of nanoclusters, and scanning tunneling microscopy (STM) has been applied to several model systems,[21–26] but the requirement of a conducting sample has restricted the STM's access to the important class of insulating surfaces. In principle dynamic scanning force microscopy (dynamic SFM)[27–29] offers the capability of imaging both the adsorbed metal clusters and the insulating surface in atomic resolution, hence providing unprecedented information about the cluster structural properties. However, very few attempts have been made to image these kinds of systems in dynamic SFM,[30–35] mainly due to the technique's slower development compared to STM. A recent dynamic SFM study on gold clusters adsorbed onto the (001) KBr surface[33] was able to obtain atomic resolution on the surface, but, crucially, could not resolve the clusters at a similar level. In this work, we use a combination of first principles theory and experiment to try and understand SFM imaging of Au on KBr in more detail, and hence suggest methods for improving resolution.

II. METHODS

A. Experimental method

The samples had a purity of 99.7% and were taken from commercial single crystals of KBr (Korth Kristalle GmbH). The surfaces were prepared by ultra high vacuum (UHV) cleavage at room temperature parallel to the (001) cleavage plane of KBr. All the crystals were additionally annealed in an UHV oven between 80 and 100 °C for a few hours in order to reduce charges which appear after cleavage. A detailed description of our methods for the preparation and of UHV cleavage induced charging of ionic crystals can be found in Refs. 36 and 37, respectively.

Gold clusters were epitaxially grown by condensing a calibrated beam of neutral gold atoms from a Knudsen cell onto the KBr surface at a crystal temperature of around 100 °C. For all experiments we used a constant flux of 1×10^{13} atoms/cm^2 s. No nucleation of clusters took place in the gold beam. The base pressure did not exceed 3×10^{-9} mbar during the deposition. After the deposition, the sample was cooled down to room temperature before taking measurements. The gold deposition and the measurements were taken in the same UHV system.

Experiments were performed with a dynamic SFM (Omicron STM/AFM) operated at room temperature in UHV with a base pressure in the low 10^{-10} mbar range. Dynamic SFM measures the change in frequency (detuning Δf) of an oscillating cantilever due to the interaction of a tip at the end of the cantilever with the surface.[27–29] In order to measure the detuning with highest precision and utmost stability the system is equipped with a digital demodulator (Nanosurf). P-doped silicon (1.5 Ω cm) cantilevers (Nanosensors) were excited to vibration at their resonance frequency with a peak-to-peak amplitude ($A_{p\text{-}p}$) stabilized to a few nanometers. In order to minimize electrostatic forces originating from residual surface charges, a constant bias voltage U_{dc} was applied at the rear side of the crystal.[36,37]

Imaging the (001) surface of KBr can be routinely done[36,38–40] and is usually easier than for other similar surfaces, e.g., MgO(001). In general, the tip is first approached to the surface and set to scan the surface for more than

30 min without taking images in order to wait until a major amount of creep of the scanner is reduced. Further, during this time the mean voltage for minimizing electrostatic forces due to residual charges can be determined by several Δf versus bias voltage curves at different places on the surface.[33] We then choose a spot on a large, atomically flat terrace for imaging with atomic resolution and make the preset value of Δf more negative successively from image to image. In between images with atomic resolution, a Δf versus distance curve is carried out which is important for the comparison with theory as discussed later. We applied this procedure at many places on the KBr(001) surface and got several series of images with atomic resolution. Images were produced in the constant detuning and constant height mode,[41] more details of the scanning parameters of the measurements presented here can be found further below.

B. Computational details

All calculations were carried out with the periodic SIESTA code,[42] which implements density functional theory (DFT), using GGA with the Perdew-Burke-Ernzerhof exchange-correlation functional.[43] All calculations were spin-polarized, and we used standard Troullier-Martins norm-conserving pseudopotentials to represent the core electrons, with scalar-relativistic corrections for Au. As the basis set we used double ζ with polarization for K ($4s^1$), outer Br-shell ($4p^5$) as well as inner Au shell ($5d^{10}$), double ζ for inner Br shell ($4s^2$), and triple ζ with double polarization for outer Au shell ($6s^1$). A change to double ζ with polarization as the gold basis was made for Au(001) surface simulations, as the computational cost of these calculations is heavy due to the system size of more than 100 Au atoms, but the effect on accuracy was minimal. k-point sampling was checked for the surface calculations, and a $2\times2\times1$ grid proved sufficient for KBr and the Au surface. An energy shift of 25 meV and mesh cutoff of 150 Ry were used, and unconstrained forces were relaxed below 0.02 eV/Å.

C. Tip and surface setup

The tip used for experiments is nanofabricated from p-doped silicon and carries a thin oxide layer due to a exposure to air prior to its transfer into UHV. During imaging the surface with high or atomic resolution it happens occasionally that tip changes appear at close distances. They are visible by a change of the contrast, especially in the damping image, or in that the tip oscillation breaks down due to strong tip-surface interactions. In these cases the tip frequently changes its atomic configuration due to transfer of material between tip and surface. We therefore consider the case in which the tip is covered with a small amount of material from the surface, i.e., gold or some form of KBr cluster. In order to model these possibilities we considered three different tips: A 13-atom Au minimum energy cluster[44] [see Fig. 1(a)] and two 12-atom KBr clusters, formed from $3\times2\times2$ atom cuboids [see Fig. 1(b)], with reversed atom positions and therefore with two different terminating ions, K^+ and Br^-. In all cases a small number (five or six) of atoms at the top of the tip were frozen to represent the connection to the rest of the macroscopic tip, and all other atoms were allowed to relax completely during simulations. Note that we have chosen a small, 12 atom KBr cluster in order to make the first-principles simulations manageable. Due to the small number of atoms, the tip is generally softer and shows more atomic relaxation than in previous (atomistic) simulations with a cubic 64 atom KBr cluster.[45]

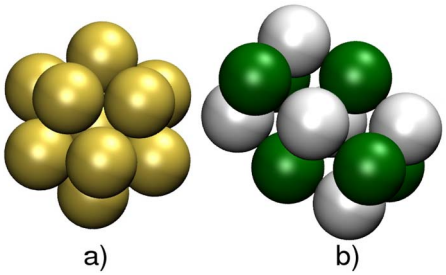

FIG. 1. (Color online) (a) Au_{13} tip and (b) $(KBr)_6$ tip used in imaging simulations. K^+ ions are represented by the green (darker) spheres.

In experiments the gold clusters on the surface are generally of the order 2–15 nm in apparent lateral size, well beyond the capability of DFT-based imaging simulations. Hence, the main criterion for our cluster selection was to provide a relatively flat, horizontal top facet, which would mimic the larger clusters in experiments. We found that a 26-atom gold cluster (10-8 potential Sutton-Chen cluster[44]), seen in Fig. 2, fulfilled this requirement if we removed one atom from it to form a flat base, and relaxed the whole clus-

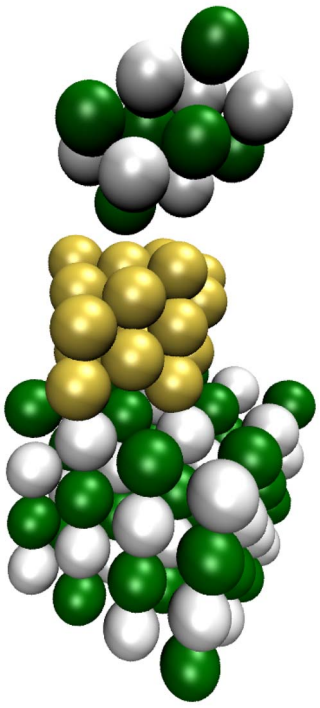

FIG. 2. (Color online) K^+-terminated $(KBr)_6$ tip imaging the 25-atom Au cluster on KBr surface. The cluster has a mean lateral size of about $d=1.1$ nm and a height of $h=0.8$ nm. K^+ ions are represented by the green (darker) spheres.

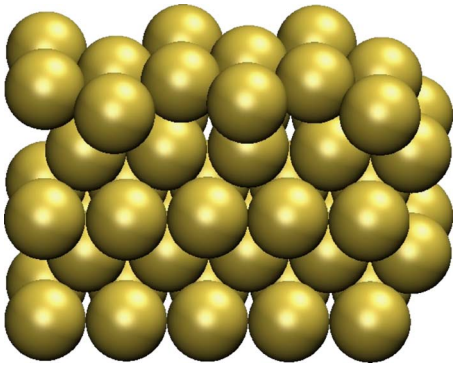

FIG. 3. (Color online) Au(001) surface structure with (1×5) reconstruction. The surface used in calculations was two times larger, having 24 atoms at the top layer oriented towards the tip.

ter on the surface—the general cluster shape does not change significantly after relaxation. Our simulations demonstrate that the specific adsorption site of the cluster onto the substrate has no significant effect on the properties of the uppermost atoms of the cluster (see Sec. IV for further discussion). Since these atoms almost exclusively determine the tip-surface interaction, we consider the cluster in Fig. 2 as a good general model of a nanometer sized gold cluster adsorbed on the KBr(001) surface. To model the imaging of larger clusters with almost no effective curvature, we also considered direct imaging of the Au (001) (1×5) surface. For larger clusters, the influence of the insulating support will be heavily screened at the surface of the cluster, and a gold surface is therefore a good model. Gold clusters are known to present both (111) and (001) facets,[46] but the difference with respect to imaging is not significant as both are effectively smooth. Hence, we use the reconstructed Au(001) surface as a model, where the uppermost layer forms hexagonal packing on top of a fcc bulk structure. The unit cell is larger than can be practically implemented in SFM simulations,[47] but it can be modeled with a rather similar (1×5) reconstruction (see Fig. 3) seen for example in Ir(001), and also initially proposed for Au(001). Our model surface includes 4×5 fcc unit cells and one 24 atom hexagonal surface layer, 104 Au atoms in total.

To represent the KBr(001) surface, a four-layer KBr slab was used, with the bottom layer atoms in fixed positions during relaxation. Tests proved that this is deep enough to restrict the relaxations of the second-lowest layer to below 0.1 Å. The size of the surface in the *x-y* direction was changed according to the process being studied. For simulating images we require a system as small as possible, while still larger than the surface Au cluster and large enough to avoid interactions between periodic images of the tip. For this we found that 4×4 surface (see Fig. 2) was sufficient. Note that this does allow some interaction between the surface gold clusters in images of different periodic simulation cells, but this does not affect the tip-surface interaction. For calculations of charge transfer to the clusters it was important to study isolated clusters on the surface, so we increased the size of the surface to either 6×4 or 6×6, depending on surface features needed in the simulation. In this way we could be sure that the cluster is well separated from its neighbors in the supercell.

D. Simulating SFM

In order to generate images which can be compared to experiment, it is also important to include the long-range macroscopic van der Waals interaction between the tip and surface. This force is effectively controlled by the radius of the tip and Hamaker constant of the system. Since the original tip is likely oxidized silicon, we fix the Hamaker constant at the value $A=6.04\times10^{-20}$ J for SiO_2 interacting with an alkali halide[48] and fit the radius to produce a match with an experimentally measured frequency change versus distance curve. In reality, the Hamaker constant will be effectively increased when the tip is over a gold cluster, but we assume that this contribution is not significant when the tip is larger than the cluster.[49] A tip radius of 4.0 nm provides a good match between experimental and theoretical frequency change versus distance curves.

Finally, the microscopic and macroscopic forces are combined to provide a total map of the force across the surface. This is then used in a simple model[50] of the cantilever oscillations (using experimental parameters) to provide a simulated image for a given constant frequency change. The simulation method described briefly here is in itself not novel, and greater detail can be found in Ref. 29. Even when it is the short-range interaction that provides the atomic contrast, the long-range forces have a large effect on determining the tip-sample separation at which the experimental frequency shift is seen, and therefore a large effect on obtained contrast. The dependency of contrast on detuning is here similar in both the experiments and the simulations, increased detuning first increases the contrast, and finally decreases as we approach repulsion. All discussed tip-surface separations are the distances between atom centers of tip apex ion and a reference atom (highest in the imaging area) in the surface or cluster. Thus the tip is "in contact" with the surface at about 3 Å separation.

III. RESULTS

A. Imaging the ideal KBr (001) surface

The KBr(001) surface has been previously simulated with atomistic calculations,[45] where theoretical force curves were compared with low-temperature experimental site-specific force curves. Although the authors did not achieve quantitative agreement, they could identify the tip used in the experiments as a K^+-terminated KBr tip by comparing the force differential curves between surface sites to experiment. The results of our *ab initio* simulations show both similar, as well different characteristics to the atomistic simulations: the range of separation where the maximum attraction is above the opposite ion is similar, however for the K^+-terminated tip the maximum attraction in our simulations is one-third stronger, whereas for the Br^--terminated tip it is one-third weaker. The different results are caused by the different computational method as well as different tip models. Compared to the larger tips of Ref. 45 our tips are less rigid and thus allow more relaxation, and our method includes also electron charge density redistribution in the tip and surface.

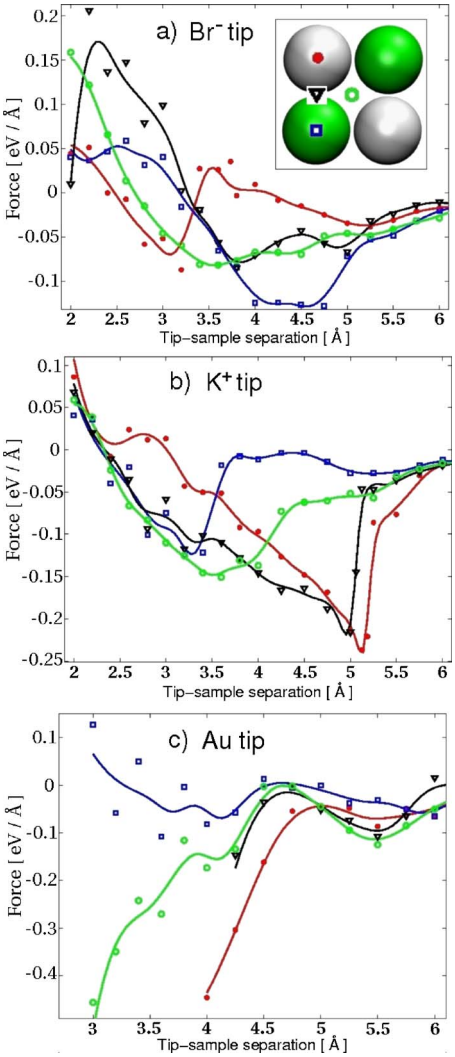

FIG. 4. (Color online) Force-distance curves over different KBr surface sites, imaged with Au and KBr tips. Br^- and K^+ tips denote Br^-- and K^+-terminated $(KBr)_6$ tips respectively. The lines are fitted averages to the calculated points of the same color. Legend (see also the inset): Red (middle gray) disks: over Br ion. Blue (dark gray) squares: over K ion. Black triangles: bridging position between K and Br. Green (light gray) circles: over the cell center.

Here we consider also the appearance of images and the interaction of a Au tip. Imaging simulations were run with all three tips above four surface sites: above a K^+ ion, above a Br^- ion, over the bridging position, and over the unit cell center (see inset in Fig. 4). The surface and tip structures were first relaxed separately, and then brought to the smallest atomic separation of 6 Å, where the first constrained relaxation and force calculation took place. At this range the surface-tip DFT force is zero within the error limits. Then the tip is sequentially moved toward the surface with steps of 0.25 Å steps, relaxing the system and calculating the force after each step. Below 4 Å tip-surface separation, we reduced the step size to provide a finer mesh. The calculated force data can then be fitted to continuous force-distance curves for all three tips above the four surface sites, as seen in Fig. 4.

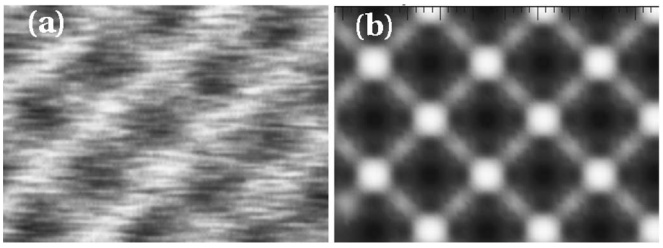

FIG. 5. (a) Experimental constant height image showing black disk with a white rim contrast. The image was additionally straightened and slightly Fourier filtered. (f_0=267.9 kHz, average Δf =−55.0 Hz, k=32 N/m, A_{p-p}=13 nm, U_{dc}=−0.02V, contrast in Δf=3.4 Hz, image size 1.9 nm×1.4 nm). (b) Simulated KBr surface imaged with a Br^--terminated KBr tip at a constant height of 4.9 Å. The parameters of the tip oscillation (f_0, Δf, k, A_{p-p}) in the simulation were the same as in the experiment.

For a Br^--terminated tip a clear force contrast is seen only below 5 Å, where the interaction over the K^+ ion is the most attractive. The interaction at the unit cell center is also significant, and produces a contrast pattern in images of a black disk with a white rim. The interaction is quite delocalized due to deformation of the tip—our smaller cuboid tip is softer than the large cube used in previous simulations,[45] and when the apex experiences a strong repulsive interaction (over like-ion sites) it bends to a more favorable configuration. Figure 5(a) shows an example of an experimental constant height image with a good qualitative agreement with theory image Fig. 5(b). In this case, Fig. 5(a) was measured just before taking a frequency change versus distance curve. The frequency change versus distance curve was used to fit the long-range part of the tip-surface interaction which is important for the simulations.[51] This allows us to make a comparison between theory and experiment—the good agreement in measured and simulated contrast found here gives us confidence that the theoretical and experimental interactions are comparable.

For a K^+-terminated tip a strong force contrast is seen already at large separation, about 5.2 Å. The site above a Br^- ion first demonstrates the largest attraction, as expected. Below 5 Å, however, the bridging position is the most attractive site, due to a slight bending of the tip toward Br from the bridging position, whereas above the Br position it is already too close to Br for maximum attraction. This agrees with the behavior seen in experimental force curves[45] at similar distances and also with atomistic simulations of a similarly terminated tip. This tip results in the *classic* white disk contrast usually associated with simple cubic crystals, and seen in other experiments.[45] Figure 6 shows a comparison between a standard disk-like image of the surface, and a simulated image produced with a K^+-terminated tip. Both images here are constant frequency shift images. We see immediately qualitative agreement in the contrast patterns. We emphasize that the difference between computational images is caused by different tip termination, the differences between constant height and constant detuning images were negligible.

For the gold tip the simulations produced images with contrast and contrast pattern similar to Fig. 6, and in principle cannot be differentiated from imaging with a

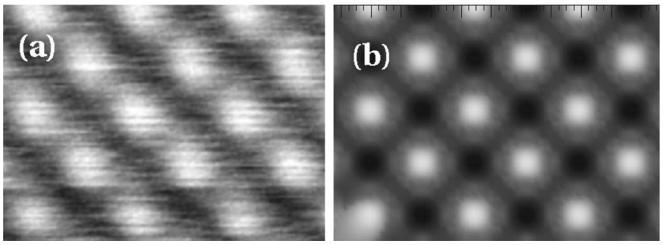

FIG. 6. (a) A typical experimental constant frequency change image of the KBr surface showing white disk contrast. The image was additionally straightened and is not filtered (f_0=293.2 kHz, Δf=−83.8 Hz, k=48.5 N/m, A_{p-p}=4.2 nm, U_{dc}=0.056 V, contrast in z=39 pm, image size 2.0 nm×1.5 nm). (b) Simulated KBr surface imaged with a K^+-terminated KBr tip with constant frequency change. Bright spots (attraction above Br^- ions) are clearly separated. The parameters of the tip oscillation (f_0, Δf, k, A_{p-p}) in the simulation were the same as in the experiment.

K^+-terminated tip. However, contrast was only achieved at a rather small imaging height, and as the gold tip was much more prone to atomic jumps due to its softness and strong interaction with Br, stable imaging is likely to be much more difficult than with an ionic tip. Two of the force curves shown in Fig. 4(c) end at about 4 Å separation because of such atomic jumps, in which the tip picks up material from the surface. Similar structural changes were encountered when simulating the imaging of gold clusters (see Sec. III B).

Although here we show that different tip terminations present characteristic contrast patterns which agree with experiment, it is important to understand that this does not provide unambiguous interpretation. Our results indicate that the black disk with a white rim contrast is almost exclusive to a Br^--terminated tip, and the white disk contrast is characteristic for a K^+-terminated tip (also in agreement with Ref. 45). However, we cannot exclude the influence of less ideal tips in the experiments.[52] Here we are merely demonstrating the general plausibility of the tip models, and more extensive efforts in interpretation require other sources of information on the tip or tip-surface interaction.[45]

B. Imaging gold clusters

Gold was deposited with a nominal thickness of 0.07 ML on a freshly prepared KBr(001) surface and formed clusters with a mean apparent lateral size of 6±1 nm and a mean apparent height of 1.7±0.6 nm. Note that the latter sizes were taken from the images without taking the influence of the tip into account so that the clusters had probably a smaller size. During the Au deposition, the substrate was held at a temperature of 100 °C in order to crystallize the clusters into a symmetric form.[53] As can be seen in Fig. 7 the clusters decorate mostly steps, which is a well-known phenomenon of gold on surfaces of alkali halides.[54,55] Only a very small number of clusters are located on terrace sites. Since gold is deposited atom-by-atom in the experiments, to identify likely cluster nucleation sites theoretically we consider the adsorption of a single Au atom on the surface, above and below step-edges, and at anion vacancies

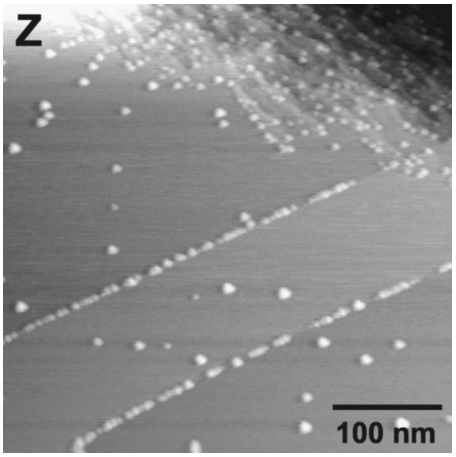

FIG. 7. Topography image of the KBr(001) surface after the deposition of 0.07 ML of gold. Note that the density of clusters directly scales with the density of steps which is lower in the lower part of the image than in the region on the top of the image (400×400 nm^2, 293.2 kHz tip, Δf=−23.9 Hz, k=48 N/m, A_{p-p}=13 nm, U_{dc}=5.0 V, contrast in z=6 nm).

(F-center F^0: vacancy with electron, F-center F^0_{gold}: F^0 filled with a gold atom) in the surface and at step-edges. The calculations show that adsorption energies for a single Au atom on the surface and inside the F-center were 0.77 and 3.90 eV, respectively, and there is no energy barrier for filling the vacancy. At step edges, we find adsorption energies of 1.18 and 1.30 eV, above and below the edge respectively, but this increases to 3.70 eV for adsorption in an F-center at the step-edge. If we compare the formation energies of an F-center at the terrace (5.4 eV) and at a step-edge (4.8 eV), we see it is more favorable for these F^0-centers to exist at step-edges, although they are not very mobile on KBr at the maximum temperature (100 °C) of these experiments (diffusion barrier: 0.9 eV[56]). In general, the calculations predict that gold clusters are more likely to nucleate at steps, as seen in these and previous experiments.

As already pointed out before, imaging gold clusters with highest resolution is a rather difficult task.[33] Nanometer sized clusters are mostly as large as the asperity of the tip or even smaller so that the asperity of the tip strongly influences the imaging contrast due to long-range tip-cluster interactions.[33] In the extreme case, the cluster is much smaller than the tip size so that the tip is imaged rather than the cluster itself.[33] Despite these difficulties, it should be possible to obtain atomic resolution on top of the clusters with a sharp tip since in this case only the last atoms of the tip interact with the cluster and no influence of tip convolution is present. However, in all cases imaging the top of the cluster with such a resolution failed.

In Fig. 8 we exemplify what happens if a sharp and symmetric tip is successively approached to a cluster from image to image. The series of images in this figure reflect general observations also made in other series performed above other clusters. The tip-cluster distance was successively reduced by making the pre-set value of the detuning more negative after each measurement [(a)–(f)]. Alongside the topography signal (z), the residual contrast in the detuning Δf image was

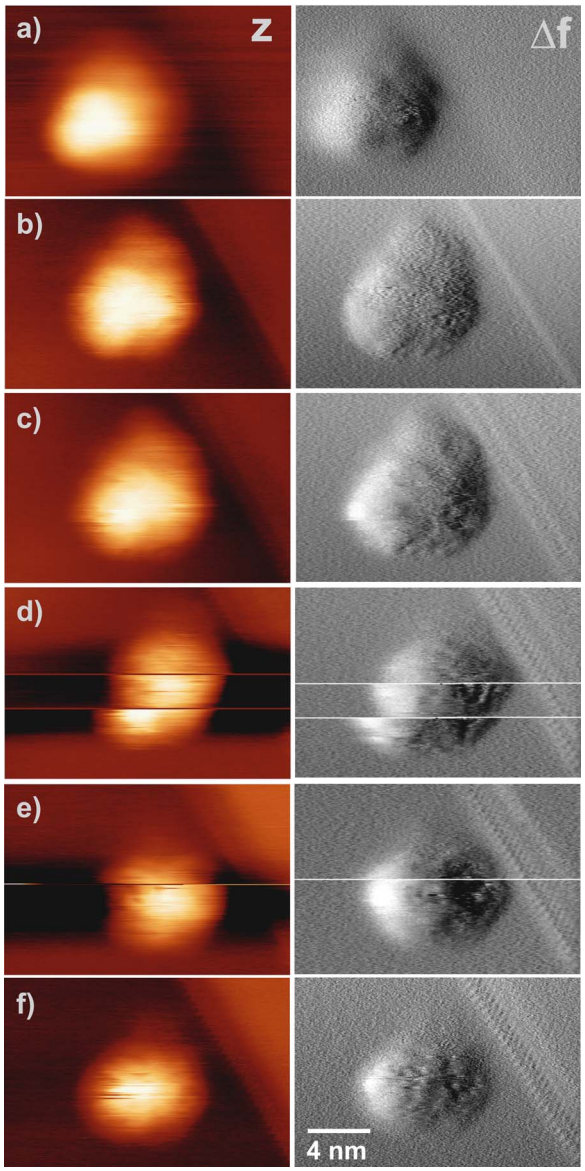

FIG. 8. (Color online) Topography (z) and detuning (Δf) images of a gold cluster taken at different distances (top→bottom: distance decreases). z-value given for each image denotes the corrugation in topography images. In detuning images the contrast is up to 15% of Δf. (18×12 nm^2, 293 kHz tip, k=48.5 N/m, A_{p-p}=10 nm, U_{dc}=0.06 V, (a) Δf=−7.7 Hz, z=1.0 nm, (b) Δf=−17.2 Hz, z=1.3 nm, (c) Δf=−23.2 Hz, z=1.5 nm, (d) Δf=−28.1 Hz, z=1.2 nm, (e) Δf=−32.3 Hz, z=1.2 nm, (f) Δf=−37.9 Hz, z=0.9 nm.)

recorded simultaneously. In the first three images [(a)–(c)] a cluster with an apparent size of 5.5 nm is shown. The cluster has a round and fuzzy appearance which does not change with distance. We assume that the cluster had probably the shape of a truncated pyramid, as expected for clusters of such sizes.[57] The threefold symmetry axis is due to (111) epitaxy which is well known at the early stages of growth of gold clusters on alkali halide surfaces.[46] No atomic contrast could be found on top of the cluster. Between measurement (d) to (e) the pre-set value of the detuning was again lowered by 5 Hz approaching the tip further to the cluster. In the middle of image (d) the tip oscillation broke down two times within a scanning line, but each time the oscillations soon stabilized and imaging could be resumed. Before recording the next image (e) the pre-set value of the detuning was again lowered by 4 Hz and another such *tip instability* occurred in image (e). After a further approach image (f) was gained without a tip instability.

The most interesting observation is that the tip instabilities in the images (d) and (e) appeared when the atomic resolution was gained at the step edge of KBr which can be best seen in the detuning images. Gaining atomic resolution on the KBr(001) surface means that the tip's last atom had a distance of only 4–5 Å (see above, and also Ref. 58) so that one can anticipate that the tip-cluster distance was also relatively small during recording images starting at (c). However, a detailed analysis of all images shows no atomic contrast details on top of the cluster. Note that we also performed measurements on the top of other clusters with a much smaller scanning frame in order to observe subtle atomic contrast features with highest resolution. These were never observed, and same characteristics of tip changes always appeared when the tip got too close to the cluster.

Another observation is that the cluster changed its shape (d) after the tip instabilities. The cluster in (d) has a rounder top than before [(a)–(c)]. Although it is impossible to find out how the cluster and/or the tip changed during the tip instabilities, it is obvious that some kind of exchange of particles occurred between tip and cluster during the tip instabilities. Further details and a discussion of the nature of tip-surface convolution when imaging nanoclusters can be found in Ref. 41.

In order to understand why we did not obtain atomic resolution on top of gold clusters, we performed simulations of the contrast formation of these type of small clusters. Imaging simulations using all three tip models were run above two sites on the Au cluster adsorbed on the KBr surface: above a gold atom and above the center of a hollow site, both in the middle of the almost horizontally aligned top facet. Tip changes and atom jumps were the major features of the gold cluster imaging simulations, similar to KBr surface imaging simulations with the Au tip discussed in the previous section.

The results of the simulations agree well with the experimental observations, with all three tips a clear contrast is missing, as explained in the following and shown in Fig. 9, showing the DFT force between the tip and cluster above two cluster surface sites. As soon as the tip-cluster distance reaches a distance of 4.5–5.0 Å, atomic contrast can be seen in principle with the the K^+ tip and the Au tip. However, the corrugation of 0.1 Å (determined from simulated frequency shifts) is too small to be detected by the force microscope, where noise measures 0.1–0.3 Å at room temperature, in most cases. Also the distance window of 0.5 Å for atomic resolution imaging is very small. The main limiting factors are, however, tip changes and atom jumps between tip and cluster which immediately occur for Br^- and Au tips as soon as the tip-cluster distance is below 4.5 Å. These structural changes were a major factor in increasing the interaction strength by bringing atoms into contact (for example, responsible for the contrast with Br^- tip below 4.2 Å), and included rearrangements of cluster atoms, displacement of the whole

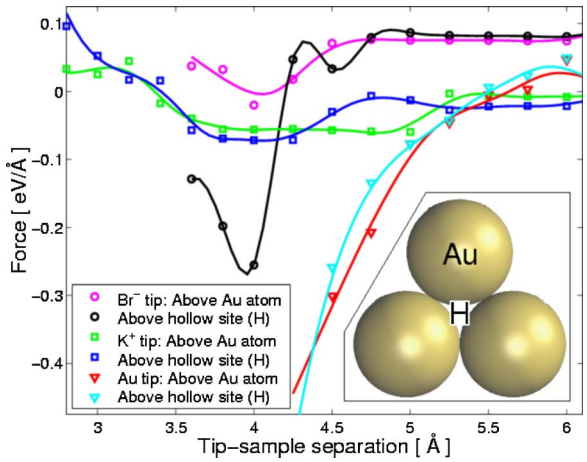

FIG. 9. (Color online) Tip-cluster forces, above two surface sites of the Au cluster. In the inset Au denotes the site directly above a gold atom, and H the hollow site between atoms. Note that the Br^- tip curves have been raised by a constant force of 0.1 eV/Å for clarity. For all three tips the force contrast between the two surface sites is small, except for the Br^- tip at 4 Å separation, where atomic jumps hinder imaging.

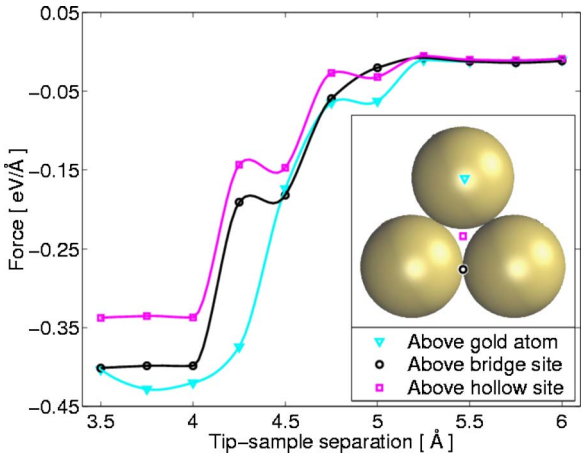

FIG. 10. (Color online) Force-distance curves above three surface sites of the reconstructed (1×5) Au(001) surface shown in Fig. 3, imaged with the Br^- terminated tip. With typical experimental imaging parameters the force contrast between most attractive and least attractive sites corresponds to a small 0.25 Å contrast in topographic images.

cluster and some surface atoms toward the tip, and reorientations of the tip with respect to the cluster. To summarize, with the K^+ tip the interaction is too weak at all distances to produce measurable contrast, and with Br^- and Au tips contrast is only available at tip-sample separations where the tip risks entering a region of instability during scanning so that structural changes of the tip-cluster system can occur. The latter modifies strongly the tip-cluster interaction, and likely provokes a tip instability as we frequently observe in our measurements (e.g., see Fig. 8 and associated discussion). The structural changes seen in simulations would also likely lead to a large dissipation signal in experiments which has been observed in other measurements (not shown).

In order to investigate the influence of the curvature and instabilities of our cluster, we also considered imaging of the Au (001) surface. For this large system we consider only simulations with a Br^--tip as this showed the largest contrast, but also the largest instabilities.

The reconstructed Au(001) surface (Fig. 3 shows half of the simulation surface) is a very densely packed and flat surface, and therefore presents much more stable SFM imaging conditions than the small cluster used in simulations. We simulate imaging above three different surface sites, and force-distance curves are obtained above all sites without large deformations of tip or surface. A small, but clear force contrast between an imaging site above gold atom and a site above empty surface site is seen in Fig. 10. Using typical experimental imaging parameters this force contrast should produce a 25 pm contrast in topographic SFM imaging, enhanced by a 24.4 pm rise of the gold atom toward the tip when the tip is directly above it. We emphasize the significance of such slight movement of surface atoms during the imaging as the primary source of atomic contrast on an otherwise very difficult monoatomic metallic surface (similar results are seen in STM imaging of gold surfaces[29]). As a conclusion, simulations predict that atomic resolution should be attainable on Au(001) surface in very careful experiments, with an electronegative (Br^--terminated) tip used representing the best possible case for obtaining resolution, whereas small gold clusters are very hard to image because they do not offer rigid flat terraces for stable scanning.

Although we have not imaged surfaces of single gold crystals so far, we believe that atomic resolution imaging should be possible in principle—images recorded in the contact mode on large gold clusters already show the periodicity of the gold lattice,[59] and true atomic resolution imaging in the dynamic mode was already shown for other metallic surfaces such as Cu(001)[60] and Ag(111).[61]

IV. CLUSTER CHARGING

As discussed in Sec. I, one of the possible explanations for the increased reactivity of small gold clusters is charge transfer from the surface (or from surface defects) to the cluster. This changes the bonding configurations of gold atoms at the cluster surface, hence greatly reducing the energy cost of critical dissociation reactions. Although KBr is not itself a relevant substrate in catalysis, the basic physics of charge transfer is likely to be similar to other insulators such as MgO, so we consider it also here.

In studies of supported gold nanoclusters two different methods of preparing clusters are generally used. Either preformed, often size-selected, clusters are soft-landed to the surface (kinetic energy <0.2 eV/atom),[13] or single atoms can be deposited on the surface, forming clusters by diffusion, nucleation, and growth on the surface, as in this study. For a cluster formed by atomic deposition we have discussed previously that they are preferentially adsorbed at steps and vacancies, and experimentally they are seen to form on the upper plane of step edges. For soft-landed Au_{25} clusters we find that they are strongly bound also to the plain surface, with an adsorption energy of 3.82 eV, and adsorption at a

TABLE I. Charge transfer from KBr surface to Au_{25} cluster [e^-] (calculated as a difference in Mulliken charges), adhesion energy of a cluster [eV], and adhesion energy of single gold atom [eV] over different surface sites. Missing values are either not calculated or not well defined.

Surface site	ΔQ (cluster)	Ead (cluster)	Ead (atom)
Plain surface	0.81	3.82	0.77
Above step edge	0.89	3.01	1.18
Below step edge			1.30
Au filled *K*-vacancy	0.37		3.20
Au filled *F*-center	1.26	4.86	
F-center	1.21	4.86	
Filled step *F*-center	1.19		3.70

step-edge is actually weaker (3.01 eV). However, as for grown clusters, adsorption at an *F*-center is still more favorable with an energy of 4.86 eV. In Table I we show the charge transfer for the 25-atom cluster, presented in Sec. II C, positioned over several different surface sites, modeling both growth modes.

The calculated values are in good agreement with previous results from other substrates.[13] Charge transfer is slightly larger at a step-edge, smaller over a cation vacancy (*V*-center) and significantly stronger over *F*-centers. The most important result obtained, was not, however, the absolute value of the charge transfer, but the different amounts of localization close to the *F*-center F^0. For a cluster positioned over a Br-vacancy filled with an Au atom, F^0_{gold}, all the extra charge transfer compared to the plain surface case lies in the substitutional atom. For a cluster positioned over an unfilled *F*-center (F^0), the charge does not localize only to the nearest atom (only +0.13 e^-), but is more widely spread in the cluster (see Fig. 11). However, the transfer is still fairly localized at the cluster-surface interface, and the atoms at the top of the cluster are not significantly affected. The charge transfer to the upper Au atoms (red +) in Fig. 11 is about −0.06 e^-, compared to over +0.3 e^- for the atoms at the interface (blue −). In general, this means that over F^0-center, the extra charge is much more available to promote reactions on the cluster surface. As we have seen that single Au atom diffusion on the KBr surface leads to the filling of F^0-centers ($F^0 \rightarrow F^0_{\text{gold}}$), cluster formation by depositing single Au atoms on the surface may lead to smaller activity than for deposition of preformed clusters. This is in contrast to the MgO (001) surface, where our calculations show that Au atoms do not fill F^0-centers due to the smaller lattice constant of MgO (2.16 vs 3.47 Å). Instead Au atoms adsorb above the F^0-centers (in agreement with previous simulations[13]), producing no reactivity dependence on the growth mechanism.

This amount of charge transfer between the *F*-center, F^0 or F^0_{gold}, and a cluster is not expected to have a notable effect on imaging the small clusters. Although in general, charging can affect topographic SFM imaging due to changes in the tip-surface interaction, in this case the charge is localized to the substrate-cluster interface and its interaction with the tip is screened by the metal cluster itself.

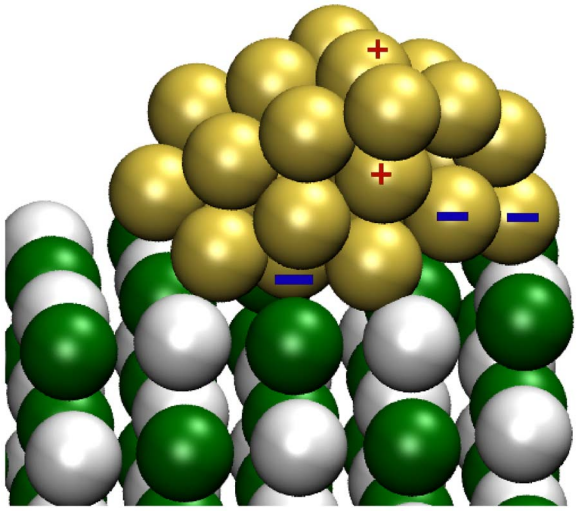

FIG. 11. (Color online) Charging in the Au_{25} cluster over an *F*-center (Br vacancy). Negative (blue −) charging in the atoms close to the surface, positive (red +) charging in the upper layers of the Au cluster. The *F*-center is below the lowest negative gold atom.

However, it is still not clear why a possible charging of large gold clusters, which contain more than 200 atoms, was observed.[33] It could be that these large clusters exhibit different electronic characteristics than clusters below 50 atoms.[62] Another likely explanation lies in a charging of the underlying insulator itself, especially at step-edges,[37] on which we will concentrate in the future.

V. CONCLUSIONS AND FUTURE STUDIES

In this work we have used a combination of dynamic SFM experiments and simulation to study in detail high-resolution imaging of Au nanoclusters adsorbed onto the (001) KBr surface. Our simulations show that for small (~1 nm) clusters, the small difference in interaction over different cluster sites and the prevalence of tip instabilities makes obtaining atomic resolution very difficult for all probable tips. This demonstrates that the lack of cluster resolution in experiments is not chance, but rather a systematic problem intrinsic to imaging these nanoscale gold clusters.

Further, our calculations suggest that for systems where the crystal Madelung potential favors adsorption of Au atoms within anion vacancies, a systematic dependence of the reactivity on the cluster growth mechanism may be observed. Assuming a dependence of surface-to-cluster charge transfer on cluster reactivity, clusters produced via atom-by-atom growth will tend to be less reactive than clusters directly deposited on the surface.

In general we have shown that while dynamic SFM can be successfully applied for high resolution studies of Au nanoclusters adsorbed on an insulating surface, providing atomic resolution on both surface and clusters remains problematic. Our results suggest some possible approaches for improving the situation:

(i) Resolving the real shape of clusters is directly related to the classic problem of tip-surface convolution. Aside from

more obvious improvements such as sharper tips, simulations and experiments suggest that constant height imaging offers better resolution of the cluster shape, on which we concentrate in a more detailed investigation.[41]

(ii) The simulations suggest that the increased stability, i.e., resistance to instabilities, of the Au (001) surface representing a large, flat cluster facet can provide atomic contrast. However, the contrast is small, dominated by atomic displacements and likely particular to an electronegative tip, providing a significant challenge for experiments.

ACKNOWLEDGMENTS

This research has been supported by the Academy of Finland Centre of Excellence Program (2000-2005), by the SURFOX project within the TEKES PINTA programme and by the European Community through the STRP GSOMEN. We are grateful to the Centre of Scientific Computing, Espoo for computational resources. Atomic structure figures were produced with Visual Molecular Dynamics.[63] CRMCN-CNRS is associated to Universities of Aix-Marseille II and III.

*Electronic address: opa@fyslab.hut.fi

[1] C. R. Henry, Surf. Sci. Rep. **31**, 231 (1998).
[2] M. Haruta, T. Kobayashi, H. Sano, and N. Yamada, Chem. Lett. **34**, 405 (1987).
[3] D. M. Cox, R. Brickman, K. Creegan, and A. Galdor, Z. Phys. D: At., Mol. Clusters **19**, 353 (1991).
[4] M. Mavrikakis, P. Stoltze, and J. K. Norskov, Catal. Lett. **64**, 101 (2000).
[5] W. T. Wallace and R. L. Whetten, J. Am. Chem. Soc. **124**, 7499 (2002).
[6] G. Mills, M. S. Gordon, and H. Metiu, Chem. Phys. Lett. **359**, 493 (2002).
[7] A. Cho, Science **299**, 1684 (2003).
[8] Y. D. Kim, M. Fischer, and G. Ganteför, Chem. Phys. Lett. **377**, 170 (2003).
[9] C. Lemire, R. Meyer, S. Shaikhutdinov, and H.-J. Freund, Angew. Chem., Int. Ed. **43**, 118 (2004).
[10] J. Guzman and B. C. Gates, J. Am. Chem. Soc. **126**, 2672 (2004).
[11] L. M. Molina, M. D. Rasmussen, and B. Hammer, J. Chem. Phys. **120**, 7673 (2004).
[12] M. S. Chen and D. W. Goodman, Science **306**, 252 (2004).
[13] B. Yoon, H. Häkkinen, U. Landman, A. S. Wörz, J. M. Antonietti, S. Abbet, K. Judai, and U. Heiz, Science **307**, 403 (2005).
[14] O. Meerson, G. Sitja, and C. R. Henry, Eur. Phys. J. D **34**, 119 (2005).
[15] C. T. Campbell, Science **306**, 234 (2004).
[16] V. Bondzie, S. C. Parker, and C. T. Campbell, Catal. Lett. **63**, 143 (1999).
[17] T. V. W. Janssens, N. Lopez, B. S. Clausen, Y. Xu, M. Mavrikakis, T. Bligaard, and J. K. Norskov, J. Catal. **223**, 232 (2004).
[18] R. Zanella, S. Giorgio, C.-H. Shin, C. R. Henry, and C. Louis, J. Catal. **222**, 357 (2004).
[19] I. N. Remediakis, N. Lopez, and J. K. Norskov, Angew. Chem. **44**, 1824 (2005).
[20] L. M. Molina and B. Hammer, Phys. Rev. Lett. **90**, 206102 (2003).
[21] A. Humbert, R. Pierrisnard, S. Sangay, C. Chapon, C. R. Henry, and C. Claeys, Europhys. Lett. **10**, 533 (1989).
[22] M. Valden, X. Lai, and D. W. Goodman, Science **281**, 1647 (1998).
[23] C. E. J. Mitchell, A. Howard, M. Carney, and R. G. Edgell, Surf. Sci. **490**, 196 (2001).
[24] N. Nilius, N. Ernst, and H.-J. Freund, Phys. Rev. B **65**, 115421 (2002).
[25] E. Wahlström, N. Lopez, R. Schaub, P. Thostrup, A. Ronnau, C. Africh, E. Laegsgaard, J. K. Norskov, and F. Besenbacher, Phys. Rev. Lett. **90**, 026101 (2003).
[26] A. Piednoir, E. Perrot, S. Granjeaud, A. Humbert, C. Chapon, and C. R. Henry, Surf. Sci. **391**, 19 (1997).
[27] S. Morita, R. Wiesendanger, and E. Meyer, *Noncontact Atomic Force Microscopy* (Springer, Berlin (2002).
[28] F. J. Giessibl, Rev. Mod. Phys. **75**, 949 (2003).
[29] W. A. Hofer, A. S. Foster, and A. L. Shluger, Rev. Mod. Phys. **75**, 1287 (2003).
[30] C. L. Pang, H. Raza, S. A. Haycock, and G. Thornton, Surf. Sci. **460**, L510 (2000).
[31] G. Haas, A. Menck, H. Brune, J. V. Barth, J. A. Venables, and K. Kern, Phys. Rev. B **61**, 11105 (2000).
[32] T. R. Ramachandran, A. Madhukar, P. Chen, and B. E. Koel, J. Vac. Sci. Technol. A **16**, 1425 (2000).
[33] C. Barth and C. R. Henry, Nanotechnology **15**, 1264 (2004).
[34] S. L. Tait, L. T. Ngo, Q. M. Yu, S. C. Fain, and C. T. Campbell, J. Chem. Phys. **122**, 64712 (2005).
[35] M. Goryl, J. J. Kolodziej, F. Krok, P. Piatkowski, B. Such, and M. Szymonski, Microelectron. Eng. **81**, 394 (2005).
[36] C. Barth, C. Claeys, and C. R. Henry, Rev. Sci. Instrum. **76**, 83907 (2005).
[37] C. Barth and C. R. Henry, Nanotechnology **17**, S155 (2006).
[38] C. Barth and C. R. Henry, Phys. Rev. Lett. **91**, 196102 (2003).
[39] C. Loppacher, R. Bennewitz, O. Pfeiffer, M. Guggisberg, M. Bammerlin, S. Schär, V. Barwich, A. Baratoff, and E. Meyer, Phys. Rev. B **62**, 13674 (2000).
[40] B. Such, J. Kolodziej, P. Czuba, P. Piatkowski, P. Struski, F. Krok, and M. Szymonski, Phys. Rev. Lett. **85**, 2621 (2000).
[41] C. Barth, O. H. Pakarinen, A. S. Foster, and C. R. Henry, Nanotechnology **17**, S128 (2006).
[42] J. M. Soler, E. Artacho, J. D. Gale, A. García, J. Junquera, P. Ordejón, and D. Sánchez-Portal, J. Phys.: Condens. Matter **14**, 2745 (2002).
[43] J. P. Perdew, K. Burke, and M. Ernzerhof, Phys. Rev. Lett. **77**, 3865 (1996).
[44] D. J. Wales, J. P. K. Doye, A. Dullweber, M. P. Hodges, F. Y. Naumkin, F. Calvo, J. Hernández-Rojas, and T. F. Middleton, The Cambridge Cluster Database, URL http://www-wales.ch.cam.ac.uk/CCD.html.
[45] R. Hoffmann, L. N. Kantorovich, A. Baratoff, H. J. Hug, and H.-J. Güntherodt, Phys. Rev. Lett. **92**, 146103 (2004).

[46] R. Kern, G. Le Lay, and J. J. Metois, in *Current Topics in Materials Science*, edited by E. Kaldis (North-Holland, Amsterdam, 1979), Vol. 3, pp. 131–419.
[47] N. Takeuchi, C. T. Chan, and K. M. Ho, Phys. Rev. B **43**, 14363 (1991).
[48] L. Bergström, Adv. Colloid Interface Sci. **70**, 125 (1997).
[49] S. C. Fain, C. A. Polwarth, S. L. Tait, C. T. Campbell, and R. H. French, Nanotechnology **17**, S121 (2006).
[50] A. I. Livshits, A. L. Shluger, A. L. Rohl, and A. S. Foster, Phys. Rev. B **59**, 2436 (1999).
[51] C. Barth, A. S. Foster, M. Reichling, and A. L. Shluger, J. Phys.: Condens. Matter **13**, 2061 (2001).
[52] R. Oja and A. S. Foster, Nanotechnology **16**, S7 (2004).
[53] S. Giorgio, C. R. Henry, C. Chapon, G. Nihoul, and J. M. Penisson, Ultramicroscopy **38**, 1 (1991).
[54] H. Bethge, in *Molecular Processes on Solid Surfaces*, edited by E. Drauglis, R. D. Gretz, and R. I. Jaffee (McGraw-Hill, New York, 1968), pp. 569–589.
[55] K. Yamamoto, T. Iijima, T. Kunishi, K. Fuwa, and T. Osaka, J. Cryst. Growth **94**, 629 (1989).
[56] W. Hayes and A. M. Stoneham, *Defects and Defect Processes in Nonmetallic Solids* (Wiley-Interscience, New York, 1984).
[57] S. Giorgio, C. Chapon, C. R. Henry, G. Nihoul, and J. M. Penisson, Philos. Mag. A **64**, 87 (1991).
[58] R. Bennewitz, A. S. Foster, L. N. Kantorovich, M. Bammerlin, Ch. Loppacher, S. Schär, M. Guggisberg, E. Meyer, and A. L. Shluger, Phys. Rev. B **62**, 2074 (2000).
[59] S. Ferrero, A. Piednoir and C. R. Henry, Nano Lett. **1**, 227 (2001).
[60] C. Loppacher, M. Bammerlin, M. Guggisberg, S. Schär, R. Bennewitz, A. Baratoff, E. Meyer, and H.-J. Güntherodt, Phys. Rev. B **62**, 16944 (2000).
[61] S. Orisaka, T. Minobe, T. Uchihashi, Y. Sugawara, and S. Morita, Appl. Surf. Sci. **140**, 243 (1999).
[62] K. J. Taylor, C. L. Pettitte-Hall, O. Cheshnovsky, and R. E. Smalley, J. Chem. Phys. **96**, 3319 (1992).
[63] W. Humphrey, A. Dalke, and K. Schulten, J. Mol. Graphics **14**, 33 (1996).